Inorganic Chemistry
Article
Cite This: Inorg. Chem. XXXX, XXX, XXX−XXX
pubs.acs.org/IC

Synthesis of Gold(I) Complexes Containing Cinnamide: In Vitro Evaluation of Anticancer Activity in 2D and 3D Spheroidal Models of Melanoma and In Vivo Angiogenesis

V. Ganga Reddy,[†] T. Srinivasa Reddy,*[,†] Steven H. Privér,[†] Yutao Bai,[‡] Shweta Mishra,[§] Donald Wlodkowic,[‡] Nedaossadat Mirzadeh,*[,†] and Suresh Bhargava*[,†]

[†]Centre for Advanced Materials & Industrial Chemistry, School of Science, RMIT University, G.P.O. Box 2476, Melbourne 3001, Australia

[‡]Phenomics Laboratory, School of Science, RMIT University, Plenty Road, P.O. Box 71, Bundoora, Victoria 3083, Australia

[§]School of Pharmacy, Devi Ahilya Vishwavidyalaya, Takshila Parisar, Indore, Madhya Pradesh 452 001, India

Supporting Information

ABSTRACT: A series of alkynylgold(I) phosphine complexes containing methoxy-substituted cinnamide moieties (**3a−3c** and **4a−4c**) have been synthesized and characterized. All of the synthesized complexes were evaluated for their cytotoxicity against three human cancer cell lines A549 (lung), D24 (melanoma), and HT1080 (fibrosarcoma) and the human embryonic kidney 293 cell line (Hek293T) as a proxy model for noncancer cells. Most of the synthesized compounds showed antiproliferative activity against cancer cell lines at low micromolar concentrations. Among these, complex **3c** showed a broad spectrum of anticancer activity with IC_{50} values in the range of 1.53−6.05 μM against all tested cancer lines. Complex **3c** possessed 20 times higher cytotoxicity than the reference drug cisplatin against D24 melanoma cells and showed significant anticancer activity in 3D spheroidal models of melanoma cells. Mechanistic investigations of **3c** activity indicate thioredoxin reductase inhibition through steric and hydrogen-bonding interactions, followed by the induction of oxidative stress and a mitochondrial pathway of cell death. Compound **3c** also showed significant antiangiogenic properties in a transgenic zebrafish Tg(fli1a:EGFP) in vivo model.

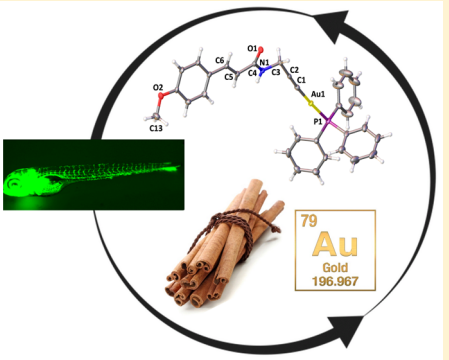

INTRODUCTION

The incidence of cancer worldwide is increasing, with 9.6 million deaths in 2018 according to World Health Organization statistics.[1] Despite the presence of existing clinical metal compounds (such as cisplatin, a platinum-based cancer drug), further developments in the formulation of metal-based drugs are necessary to overcome their high toxicity, which result in unwanted side effects.[2,3] The development of gold-based therapeutic chemistry has emerged as a promising new class of metal compounds in cancer therapy.[4−6] However, the poor bioavailability and lipophilic nature of gold complexes remain as challenges for their successful clinical translation.

The incorporation of methoxy substituents into the molecular framework of gold complexes has been shown recently to be effective in balancing the lipophilicity and hydrophilicity of the compound, a key factor responsible for cellular uptake, pharmacokinetic properties, and intracellular distribution.[7,8] Furthermore, such modification can positively influence the anticancer properties.[9]

Various synthetic strategies have been adopted in developing new gold molecules with enhanced anticancer properties and bioavailability. One such strategy is combining the properties of gold with other biologically active molecules through a molecular hybridization approach. The facile coordination of a gold-containing moiety to a biologically active molecule via a propargyl group has been previously reported. In these studies, gold complexes **A−C** (Figure 1) containing bioactive chloroquine (used in the treatment of malaria) or flavonoids (known for their antioxidant and anticancer properties) have been prepared and their anticancer activities investigated.[10,11]

In this work, a similar approach has been followed to develop gold complexes containing a cinnamide moiety

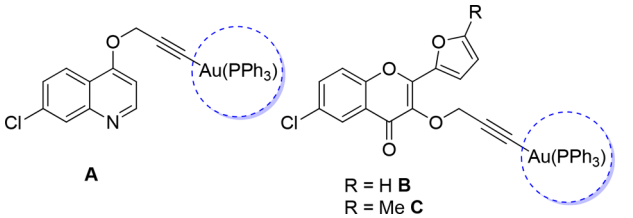

Figure 1. Gold complexes containing bioactive chloroquine (**A**) and flavonoids (**B** and **C**).

Received: January 31, 2019

DOI: 10.1021/acs.inorgchem.9b00281
Inorg. Chem. XXXX, XXX, XXX−XXX

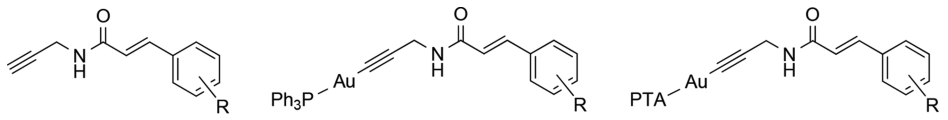

Figure 2. Structures of the methoxy-substituted cinnamide compounds and their gold phosphine containing derivatives used in this investigation.

Scheme 1. Synthesis of Gold(I) Phosphine Complexes (3a−3c and 4a−4c) Containing Methoxy-Substituted Cinnamide

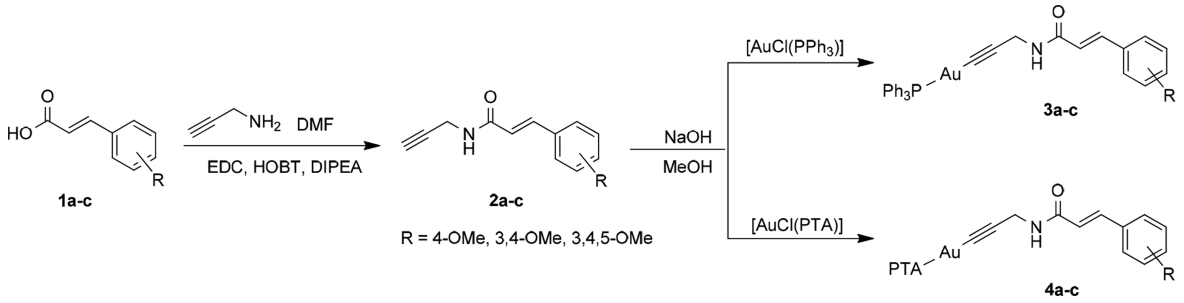

(Figure 2). Bioactive cinnamic acid derivatives are known for their medicinal applications including their anticancer potentials, which, although promising, have largely remained underutilized. Generally, cinnamic acids are often employed as an active moiety to enhance the anticancer activity of several natural products such as tallimustine, howiinol A, and acronycine, which already possess some anticancer properties.[12] This cinnamoylation approach to enhancing the anticancer activity of natural products and synthetic molecules is well documented.[13−16] For instance, trimethoxyrescinnamate is better than reserpine in its efficacy in apoptosis induction in cancer cells. In addition, introduction of the trimethoxycinnamoyl functionality to fumagillin, a natural product isolated from Asparagus fumagitis, leads to a compound (CKD731) with 1000-fold more potent cancer cell growth inhibitory activity than the parent compound. In spite of its rich medicinal significance, cinnamoylation of metal complexes and their anticancer potentials has yet to be explored. Therefore, for the first time, we have linked gold(I) phosphine moieties with propargylated cinnamides to investigate the effect of cinnamoylation on the anticancer effects of the resulting metal complexes.

To investigate the role of the cinnamide alkynes in the biological spectrum of the gold species, a range of mono-, di-, and trimethoxy-substituted cinnamides were used. We also chose lipophilic (PPh_3) and hydrophilic (PTA = 1,3,5-triaza-7-phosphaadamantane) phosphine ligands to study the effect of water solubility on the anticancer activities of this novel class of gold complexes.

Herein, we report the synthesis of six gold(I) alkyne compounds containing methoxy-substituted cinnamide moieties (Figure 2), along with their luminescent and anticancer properties and their mechanism of action.

RESULTS AND DISCUSSION

Synthesis of Gold Complexes. The propargylated cinnamides **2a−2c** were synthesized according to a previously reported method by reacting propargylamine with the corresponding cinnamic acids (**1a−1c**) in the presence of *N*-[3-(dimethylamino)propyl]-*N*′-ethylcarbodiimide hydrochloride (EDC), 1-hydroxybenzotriazole (HOBT), and *N*,*N*-diisopropylethylamine (DIPEA) under a nitrogen atmosphere.[17] Reactions of **2a−2c** with [AuCl(PPh_3)] or [AuCl(PTA)] under basic conditions conveniently give the desired air- and moisture-stable gold(I) complexes **3a−3c** and **4a−4c**, respectively, as shown in Scheme 1. The newly synthesized compounds were characterized by multinuclear NMR spectroscopy (Figures S1−S15) and, in the case of **3a**, by X-ray crystallography.

Formation of the gold alkyne complexes **3a−3c** and **4a−4c** was indicated by the disappearance of the terminal proton (δ 2.0−2.2) in the ^{1}H NMR spectra. Complexes **3a−3c** each show a singlet resonance in their ^{31}P NMR spectrum at about at δ 40 and the PTA analogues **4a−4c** at about δ −51. The structure of **3a** was also confirmed by X-ray diffraction. The molecular structure of **3a** is shown in Figure 3, with the selected bond lengths and angles in the caption. As expected, the gold atom in **3a** is approximately linearly coordinated, and the Au−P [2.2737(12) Å] and Au−C [1.986(4) Å] bond lengths are similar to those in the gold alkynyl complexes **B**

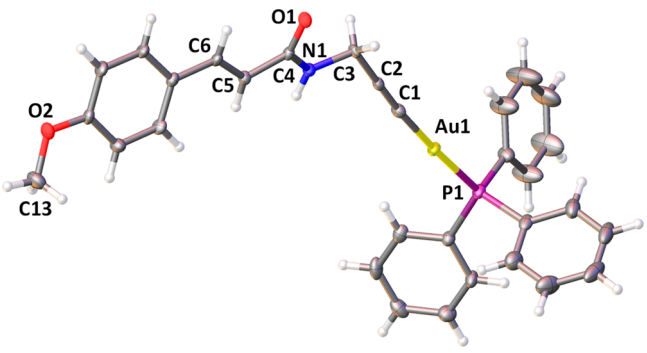

Figure 3. Molecular structure of **3a**. Ellipsoids show 50% probability levels. Selected bond lengths (Å) and angles (deg): Au1−P1 2.2737(12), Au1−C1 1.986(4), C1−C2 1.215(6), C2−C3 1.466(6), C3−N1 1.460(5), N1−C4 1.340(5), C4−C5 1.480(6), C5−C6 1.340(6), O1−C4 1.239(5), O2−C13 1.420(6); P1−Au1−C1 176.38(13), C2−C3−N1 111.5(4), C3−N1−C4 120.0(4).

DOI: 10.1021/acs.inorgchem.9b00281
Inorg. Chem. XXXX, XXX, XXX−XXX

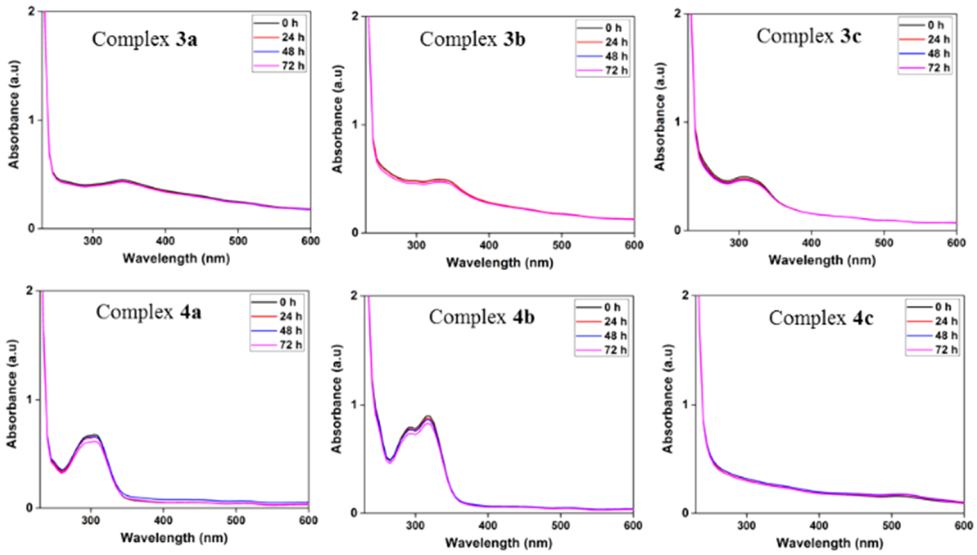

Figure 4. Electronic absorption spectra of complexes **3a−3c** and **4a−4c** (30 μM) in Tris-buffered saline (50 mM Tris, 4 mM NaCl, pH 7.4) over a period of 72 h.

Table 1. Antiproliferative Activity of Alkynes (2a−2c) and Gold(I) Alkynyl Complexes (3a−3c and 4a−4c) Expressed as IC_{50} Values (μM) Obtained from Three Independent Experiments

compound	A549 (lung)	D24 (melanoma)	HT1080 (fibrosarcoma)	Hek293T (normal)
2a	>25	>25	>25	>25
2b	>25	>25	>25	>25
2c	>25	>25	>25	>25
3a	15.5 ± 1.16	2.46 ± 0.31	2.01 ± 0.12	8.14 ± 0.86
3b	10.61 ± 1.77	2.3 ± 0.15	3.42 ± 0.26	7.25 ± 1.24
3c	6.05 ± 0.21	1.53 ± 0.12	1.62 ± 0.31	7.51 ± 0.57
4a	>25	13.59 ± 0.65	6.59 ± 0.35	11.46 ± 1.17
4b	>25	17.32 ± 2.52	10.44 ± 0.68	9.88 ± 0.32
4c	>25	8.93 ± 0.78	3.96 ± 0.34	4.67 ± 0.37
[AuCl(PPh_3)]	18.9 ± 2.31	7.90 ± 0.56	3.89 ± 0.23	3.36 ± 0.32
[AuCl(PTA)]	>25	14.67 ± 2.65	10.65 ± 1.13	8.96 ± 0.87
cisplatin	5.69 ± 0.38	23.5 ± 1.68	0.63 ± 0.12	4.78 ± 0.58

[2.2795(6) and 1.998(2) Å, respectively] and **C** [2.2829(6) and 2.001(2) Å, respectively].[11]

Stability in Dimethyl Sulfoxide (DMSO) and Physiological-like Conditions. To investigate the stability of the synthesized gold complexes, the ^{31}P NMR spectra of complexes **3a−3c** and **4a−4c** in DMSO-d_6 were measured over a period of 72 h. From the results, no significant changes were observed in the spectra, indicating that the complexes did not undergo any reduction or participate in ligand-exchange reactions with DMSO-d_6 (Figures S16−S21). The stability of the complexes was also monitored under physiological-like conditions in a buffer solution (50 mM Tris, 4 mM NaCl, pH 7.4) over 72 h using UV−vis spectroscopy. As shown in Figure 4, no significant time-dependent spectral changes were observed in the electronic spectra of complexes **3a−3c**, **4a**, and **4b**, indicating that the complexes were stable under physiological-like conditions. Complex **4c** did not show the characteristic absorbance peak between 300 and 340 nm attributed to electronic transitions of the alkyne to gold(I), but the presence of an absorbance peak at 520 nm suggests reduction of the complex to colloidal gold.

In Vitro Cytotoxicity. Proliferation assays for the alkyne compounds **2a−2c**, gold precursors [AuCl(PPh_3)] and [AuCl(PTA)], and gold(I) alkynyl complexes **3a−3c** and **4a−4c** toward A549 (lung), D24 (melanoma), and HT1080 (fibrosarcoma) cancer cells were carried out using MTT assay. Cisplatin was used as a positive control. As shown in Table 1, the gold(I) complexes **3a−3c** and **4a−4c** triggered strong cytotoxic effects, whereas [AuCl(PPh_3)] and [AuCl(PTA)] only showed moderate activity and the free alkynes **2a−2c** were inactive. These results clearly indicate that the gold(I) alkynyl fragment enhances the anticancer activity in this series of molecules. The triphenylphosphine-containing complexes **3a−3c** displayed cell growth inhibition effects in all three tested cancer cell lines, with IC_{50} values in the low micromolar range (1.53−15.5 μM). The IC_{50} values of gold complex **3c** were better than those for a series of recently studied gold(I) alkynyl complexes, which showed growth inhibition values in the range of 2.65−51.78 μM against different cancer cells.[18−21] Compound **3c** was the most active complex in the series and exhibited a 15-fold higher cytotoxicity than cisplatin against D24 melanoma cells. The gold complexes containing the water-soluble PTA ligand (**4a−4c**) were moderately active toward D24 and HT1080 cancer cells, with IC_{50} values in the range 3.96−17.32 μM. The cytotoxicity of the compounds was also influenced by the number of methoxy groups present in the alkyne moiety. Complexes **3c** and **4c** containing three methoxy substituents showed the highest toxicity toward

DOI: 10.1021/acs.inorgchem.9b00281
Inorg. Chem. XXXX, XXX, XXX−XXX

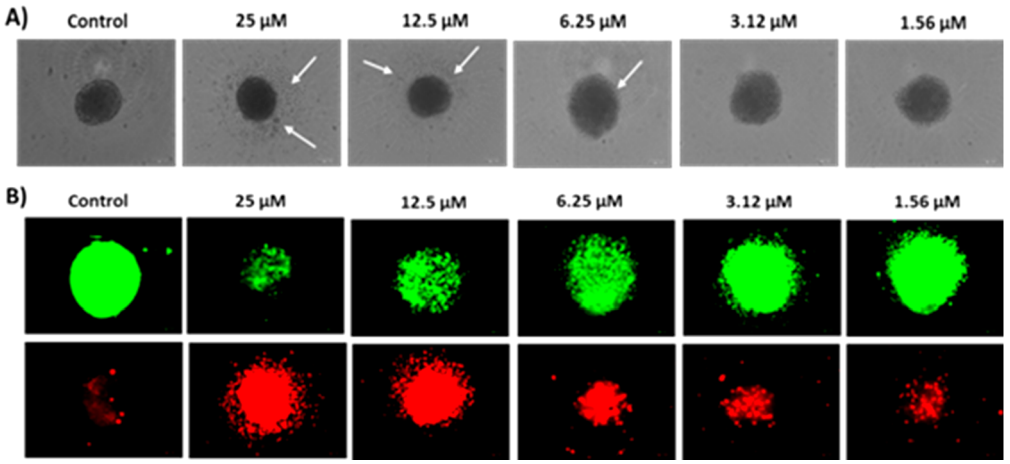

Figure 5. Antitumor activity of **3c** on 3D cellular spheroids of D24 cancer cells. (A) Cellular spheroids formed in 96-well plates treated with **3c** for 3 days examined using phase-contrast light microscopy. The arrows indicate areas of extensive disaggregation. (B) Representative images of calcein AM (live)/propidium iodide (dead) staining on D24 MCSs after treatment with different concentrations of the gold complex **3c**.

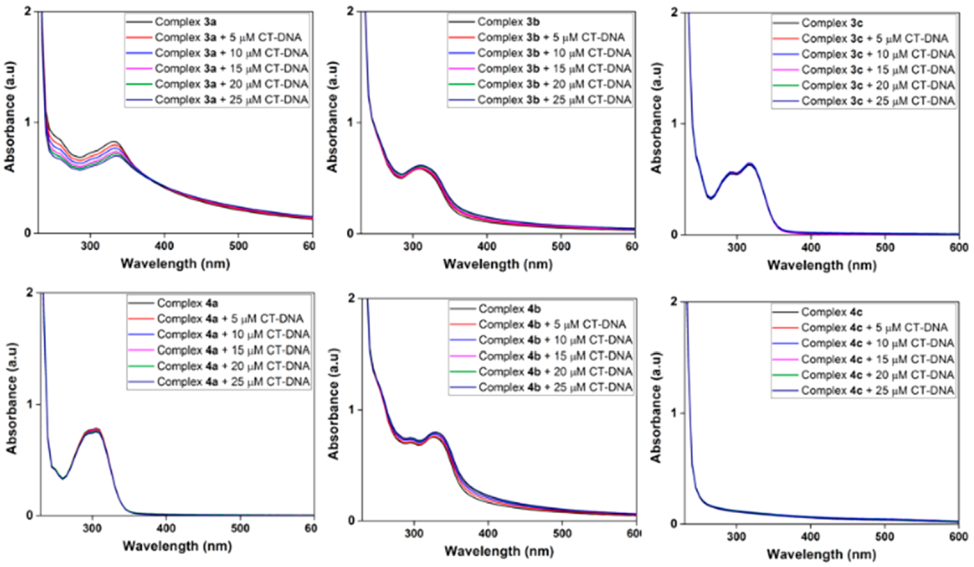

Figure 6. Electronic absorption spectra of gold(I) alkynes **3a**−**3c** and **4a**−**4c** in the presence of increasing concentrations of CT-DNA (0−25 μM).

cancer cells compared to those containing only one (**3a** and **4a**) or two (**3b** and **4b**). The results from the proliferation assays using human embryonic kidney cells indicated that the newly synthesized compounds were moderately selective toward tumor cells. For instance, complex **3c**, the most active compound among the series, displayed 5 times more selective cytotoxicity toward D24 and HT1080 cells compared to Hek293T cells.

3D Tumor Spheroidal Models. Tumor 3D spheroidal models are considered better models for drug efficacy testing than 2D monolayer cells because spheroids mimic to some degree in vivo solid tumors with respect to the development of an extracellular matrix, metabolism, nutritional concentration gradients (oxygen and glucose), and outer layer to core cell proliferation.[22,23] These models also demonstrate higher drug resistance and tumor-like penetration of drug molecules. Herein, we investigated the cytotoxicity of the most active compound **3c** in D24 spheroids. Spheroids formed over 24 h of incubation in 96-well Corning spheroidal microplates were untreated or treated with different concentrations of the gold complex for 3 days and examined for growth inhibition using phase-contrast microscopy. As shown in Figure 5A, the treatment with **3c** led to disruption and disaggregation of the spheroidal structure of D24 melanoma tumors in a concentration-dependent manner, with extensive disaggregation at concentrations of 25 and 12.5 μM. Because the spheroids were significantly disaggregated by the complex, the survival conditions, following drug treatment, were investigated using a live/dead viability assay. In this assay, the intracellular esterases in living cells convert nonfluorescent cell-permeant calcein AM into green fluorescent calcein. In contrast, propidium iodide can only enter dead cells and emits 20-fold higher fluorescence upon binding with nucleic acids. As shown in Figure 5B, untreated spheroids emitted steady green fluorescence from the live cells. However, the green fluorescence was significantly weakened, and bright-red fluorescence was observed when the spheroids were treated with 12.5 and 25 μM concentrations of **3c**, indicating that severe cell damage had occurred. These results revealed that complex **3c** induced cell death in a dose-dependent manner in a 3D spheroidal culture.

DOI: 10.1021/acs.inorgchem.9b00281
Inorg. Chem. XXXX, XXX, XXX−XXX

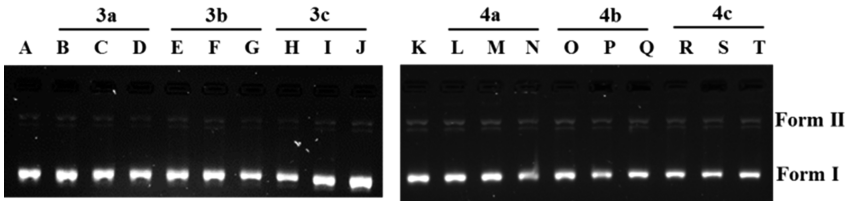

Figure 7. DNA cleavage study of plasmid PBr322 (300 ng) with varying amounts of **3a**−**3c** and **4a**−**4c** (1, 5, and 10 μM). The incubation was performed at 37 °C for 1 h, and the gel electrophoresed. The gel was then stained with SYBR safe for 30 min and photographed under UV light. Lanes A and K: PBr322 DNA (15 ng). Lanes B−D: DNA + 1, 5, and 10 μM **3a**, respectively. Lanes E−G: 1, 5, and 10 μM **3b**, respectively. Lanes H−J: 1, 5, and 10 μM **3c**, respectively. Lanes L−N: 1, 5, and 10 μM **4a**, respectively. Lanes O−Q: 1, 5, and 10 μM **4b**, respectively. Lanes R−T: 1, 5, and 10 μM **4c**, respectively.

DNA Binding Properties. To understand the interactions between the synthesized gold complexes and DNA, the UV−vis spectra of 25 μM solutions of **3a**−**3c** and **4a**−**4c** were recorded in the absence and presence of increasing amounts of calf-thymus DNA (CT-DNA; 5−25 μM). From the obtained electronic spectral data (Figure 6), no significant changes in the absorbance were observed for any of the complexes in the presence of increasing concentrations of DNA except for **3a**. In this case, a slight decrease in the absorbance (hypochromism) with an increase in the DNA concentration was observed, indicating that the complex binds to DNA through intercalation involving interactions between aromatic chromophores and DNA base pairs.

DNA Cleavage Studies. It has been established that metal ions can activate and initiate DNA endonucleolytic cleavage reactions.[24,25] Therefore, the nuclease activity of the gold(I) alkynes was investigated using pBR322, a supercoiled plasmid DNA. In agarose gel electrophoresis, the naturally occurring supercoiled DNA (form I) moves faster than the relaxed open-circular DNA (form II), also known as a nicked circular form of DNA, whereas a linear form of DNA (form III), obtained from the cleavage of both DNA strands, can migrate between forms I and II. In this study, different concentrations of gold(I) alkynes (1, 5, and 10 μM) were incubated with pBR322 DNA and agarose gel electrophoresis was carried out. As shown in Figure 7, complexes **3a**−**3c** and **4a**−**4c** showed minor or no cleavage activity under the conditions adopted in this study.

Thioredoxin Reductase (TrxR) Inhibition. It has been reported that TrxR represents a critical pharmacological target for gold(I) complexes, and its overexpression in many tumor cell lines is associated with poor cancer cell prognosis and drug resistance.[5,26] Therefore, we investigated the TrxR inhibition ability of the gold(I) alkynes to determine possible relationships between the TrxR activity and their cytotoxicity. In this assay, we also used structurally and functionally similar glutathione reductase (GR) as a reference enzyme besides the target enzyme TrxR to determine the specificity of the enzyme inhibition. The difference between TrxR and GR is the presence of a cysteine fragment in the active site of GR, whereas TrxR contains a selenocysteine fragment. Therefore, a selective TrxR inhibitor would react with the selenolate in TrxR and trigger lower inhibition against GR. The results, shown in Table 2, indicated that the gold(I) alkynes **3a**−**3c** exhibited significant TrxR inhibitory activity with EC_{50} values of 0.19−0.28 μM, whereas **4a**−**4c** showed moderate inhibition with EC_{50} values of 0.85−2.45 μM. Further, compounds **3a**−**3c** had higher selectivity toward TrxR (4.8−13.9-fold) with moderate activity on GR.

Molecular Docking. To better understand the binding modes of compounds **3a**−**3c** and **4a**−**4c** with TrxR, we carried out a docking study with the crystallographic structure of TrxR (PDB code: 2J3N). A selenocysteine residue present at the C-terminal active site is essential for catalysis. The C and N terminals are the flexible ends and the redox centers are reactive toward electrophilic inhibitors, thus demonstrating a target for antitumor drug development. It has been reported that gold complexes inhibit TrxR by binding in the cavity between the C- and N-terminal active sites.[27]

Table 2. TrxR Inhibition Activity (EC_{50}, μM) of Gold(I) Alkynes 3a−3c and 4a−4c

compound	TrxR	GR	selectivity GR/TrxR (*x*-fold)
3a	0.28 ± 0.05	1.36 ± 0.07	4.8
3b	0.21 ± 0.08	2.93 ± 0.14	13.9
3c	0.19 ± 0.03	2.16 ± 0.08	11.3
4a	0.85 ± 0.12	1.87 ± 0.23	2.2
4b	1.64 ± 0.18	5.67 ± 0.36	3.4
4c	2.45 ± 0.09	2.62 ± 0.44	1.0

As shown in Figure 8 and Table 3, all of the compounds bind in a similar mode with the TrxR enzyme at the principal catalytic site through steric and hydrogen-bonding interactions. The lipophilic compounds **3a**−**3c** showed the best TrxR inhibitory activity, indicated by the high moldock score (−159.76 to −157.79) compared to compounds **4a**−**4c** (−117.58 to −108.66) containing the water-soluble PTA ligand. These results, together with the biological experiments, suggest that the compounds' cytotoxicity is through TrxR inhibition.

Reactive Oxygen Species (ROS). Recent reports suggest that ROS (superoxide, hydrogen peroxide, and hydroxyl radicals) play a major role in the mechanism of many anticancer drugs through the initiation of programmed cell death pathways.[28,29] Inhibition of the antioxidant enzyme TrxR may result in increased ROS accumulation, leading to DNA damage and apoptosis in cancer cells.[30] Therefore, we determined the intracellular ROS levels in D24 cells after treatment with different concentrations of complex **3c** using the ROS indicator 6-carboxy-2′,7′-dichlorodihydrofluorescein diacetate (carboxy-H_2DCFDA). As shown in Figure 9, treatment with 1, 2, and 4 μM complex **3c** in D24 melanoma cells resulted in 1.5-, 2.3-, and 3.1-fold increases, respectively, of ROS production compared to the control samples. These data indicate the involvement of ROS-mediated cell death after treatment with complex **3c**.

Dissipation of the Mitochondrial Membrane Potential. Dissipation of the mitochondrial potential is known to occur at the early stages of apoptosis. Enhanced ROS generation can cause oxidative stress, thereby leading to altered mitochondrial membrane potentials.[31] The effect of

DOI: 10.1021/acs.inorgchem.9b00281
Inorg. Chem. XXXX, XXX, XXX−XXX

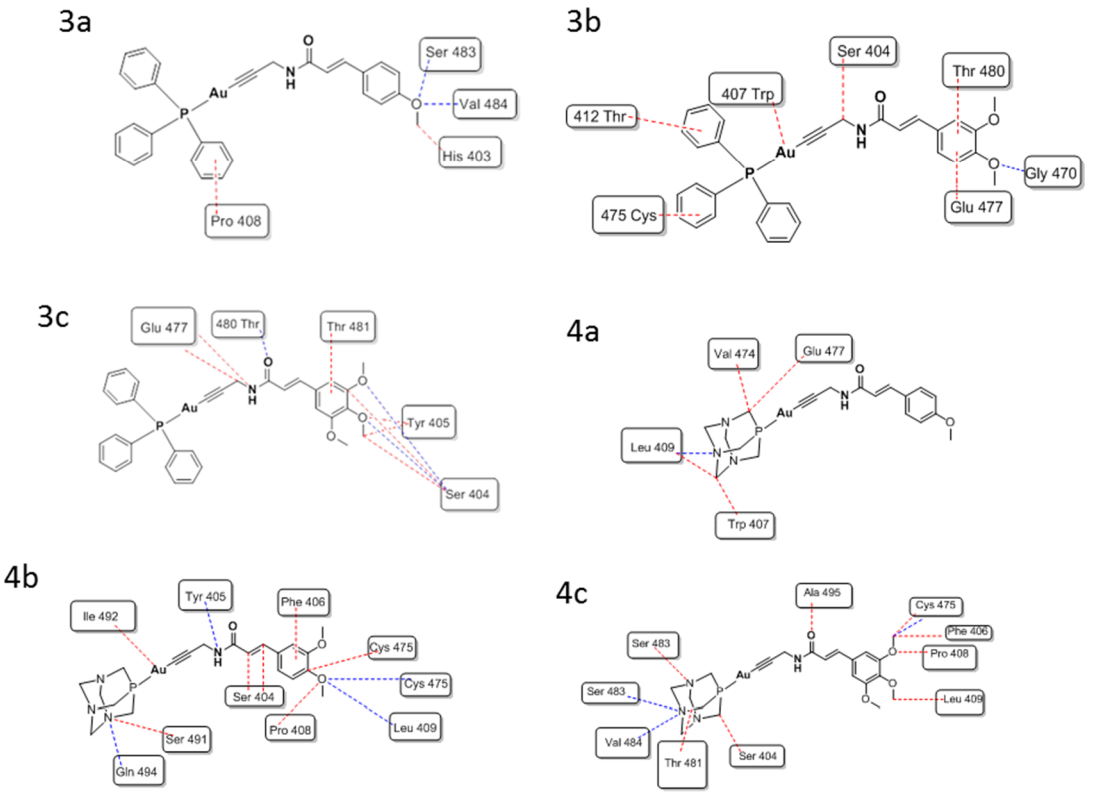

Figure 8. Pose orientation and binding interaction of **3a–3c** and **4a–4c** with TrxR (PDB code: 2J3N). Red denotes steric interactions and blue hydrogen-bonding interactions.

Table 3. Docking Scores and Interactions of Compounds 3a–3c and 4a–4c with TrxR

compound	docking score (kcal mol^{-1})	steric interactions	hydrogen-bonding interactions
3a	−159.76	Pro 408, His 403	Ser 483, Val 484
3b	−158.58	Thr 412, Cys 475, Trp 407, Ser 404, Thr 480, Glu 477	Gly 470
3c	−157.79	Glu 477, Thr 481, Tyr 405, Ser 404	Thr 480, Tyr 405, Ser 404
4a	−117.58	Leu 409, Trp 407, Val 474, Glu 477	Leu 409
4b	−110.56	Ser 491, Ile 492, Ser 404, Phe 406, Cys 475, Pro 408	Gln 494, Tyr 405, Cys 475, Leu 409
4c	−108.66	Ser 483, Thr 481, Ser 404, Ala 494, Cys 475, Phe 406, Pro 408, Leu 409	Ser 483, Val 484, Cys 475

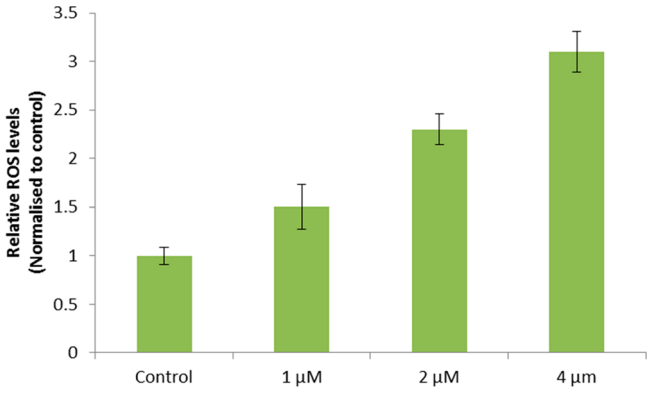

Figure 9. Effect of complex **3c** on intracellular ROS accumulation. Treated D24 cells were stained with the ROS indicator carboxy-H_2DCFDA and analyzed using flow cytometry.

complex **3c** on intracellular mitochondrial membrane potentials (DΨm) was studied using a JC-1 fluorescent ratiometric probe.[32] In this assay, JC-1-mitochondrial-specific cationic dye aggregates in the intact mitochondria and emits a red fluorescence, whereas in depolarized mitochondria, the dye forms monomers and emits a green fluorescence. Therefore, changes in the mitochondrial membrane potential during apoptosis are indicated by an increase in the green/red fluorescence ratio. As shown in Figure 10, D24 cells after treatment with complex **3c** showed a decrease in the red fluorescence and an increase in the green fluorescence in a concentration-dependent manner. These results indicate that the induction of apoptosis by **3c** is associated with a mitochondrial or intrinsic pathway.

Hoechst Staining. Apoptosis is a process of programmed cell death that plays an important role in maintaining cellular homeostasis and regular functioning of cells. Changes in the morphological features, such as nuclear fragmentation, chromatin condensation, cell shrinkage, and rupture of the cell membrane, are hallmarks of apoptotic cells.[33,34] In order to investigate the role compound **3c** plays in induced cell death, Hoechst 33242 staining was carried out on D24 cells after treatment with different concentrations of the compound for 48 h. As shown in Figure 11, the control cells were uniformly stained without any morphological changes, whereas the **3c**-treated cells were significantly more stained because of nucleus condensation. Moreover, increasing the concentration of **3c** from 1 to 4 μM resulted in a significantly higher number of apoptotic cells. As seen from the bright-field images, cell

DOI: 10.1021/acs.inorgchem.9b00281
Inorg. Chem. XXXX, XXX, XXX−XXX

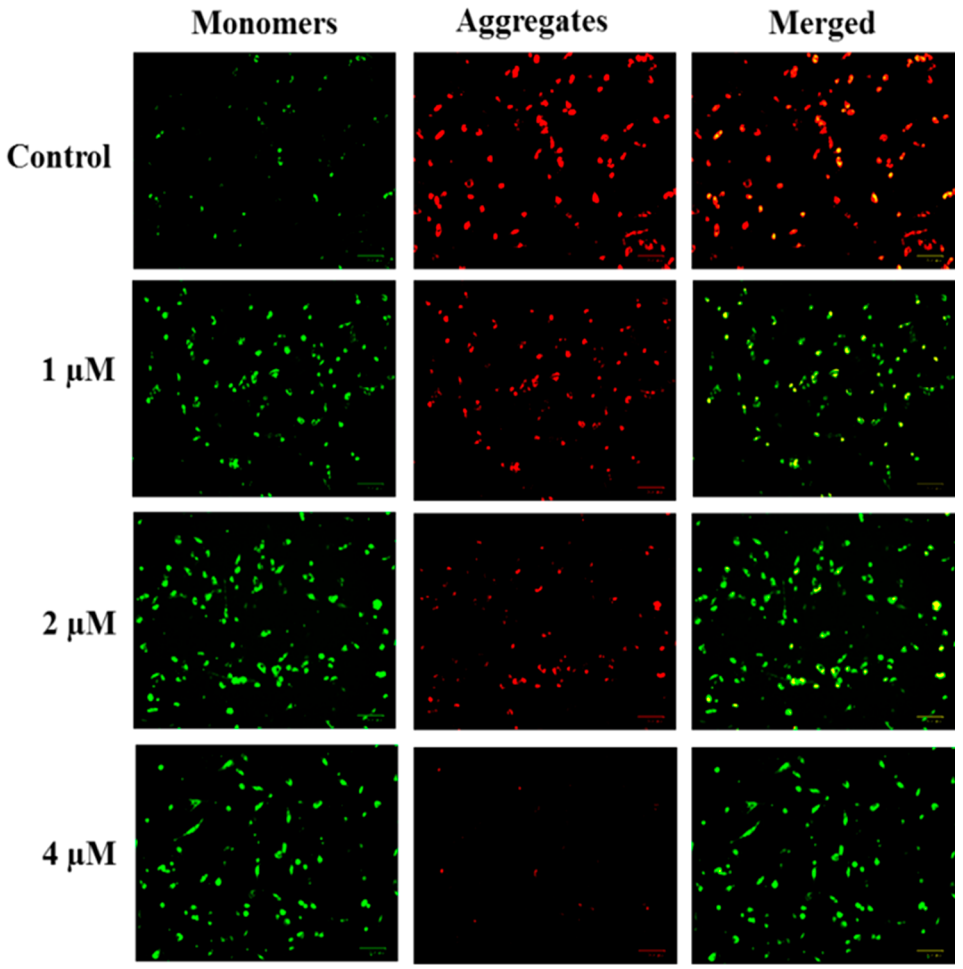

Figure 10. Effect of complex **3c** on the mitochondrial membrane potential. D24 cells incubated with the complex at different concentrations were stained with JC-1 and observed under a fluorescence microscope.

shrinkage was also observed after treatment with **3c**, indicating that apoptosis was involved in compound **3c**-induced cell death.

Inhibition of Angiogenesis in a Transgenic Zebrafish Model. It has been reported that TrxR inhibition could also contribute to angiogenesis inhibition apart from the inhibition of tumor growth and the induction of cancer cell death.[35] Further, gold(I) alkynyl compounds containing napthalimide ligands have a significant effect on angiogenesis inhibition.[36] Therefore, we investigated the angiogenesis-inhibiting properties of **3c** using a transgenic *Tg(fli1a:EGFP)* zebrafish model. The latter line expresses enhanced green fluorescent protein (EGFP) in endothelial cells and provides a rapid in situ biotest to visualize the development of characteristic patterns of intersegment vessels (ISVs). The biotest principles are based on the induction of dose-dependent inhibition of ISV formation, which can be microscopically visualized with the reduction of the fluorescence signal and quantified to provide dose response analysis.[37] In this assay, *Tg(fli1a:EGFP)* embryos at the 24 h postfertilization (hpf) stage, before sprouting of ISVs had begun, were exposed to concentrations of **3c** and cisplatin that did not induce any discernible phenotypic effects or embryo mortality. The embryos treated with axitinib, a pyrazole compound that displays strong kinase inhibition properties, were used as the positive controls.

As shown in Figure 12, no detectable ISV inhibition was observed in vehicle (0.1% DMSO)-treated embryos. In contrast, compound **3c** treatment resulted in the dose-dependent inhibition of ISV sprouting (highlighted with asterisks in Figure 12B′−D′). Partial inhibition of the ISV formation was observed after treatment with 0.1 μM compound **3c**, with significant inhibition after treatment with 0.25 and 0.5 μM concentrations. In contrast, cisplatin treatment resulted in minimal effects on the ISV formation (E and E′) even at higher concentration (1 μM). The positive control displayed significant inhibition at all of the tested concentrations with complete growth inhibition at 0.5 μM axitinib. Overall, these results indicate that gold(I) alkyne **3c** displayed antiangiogenic properties in a transgenic zebrafish model.

CONCLUSIONS

In summary, we have synthesized a new series of gold(I) alkynyl complexes containing methoxy-substituted cinnamide ligands and investigated their cytotoxic properties on 2D and 3D cancer models. The results showed that hybridization of tertiary phosphine gold(I) chloride with methoxy cinnamide alkynes led to higher cytotoxicity profiles on different cancer cells than their individual counterparts. Trimethoxy substitution on the cinnamide moiety appeared to be particularly advantageous (**3c** and **4c**) over the mono- and dimethoxy

DOI: 10.1021/acs.inorgchem.9b00281
Inorg. Chem. XXXX, XXX, XXX−XXX

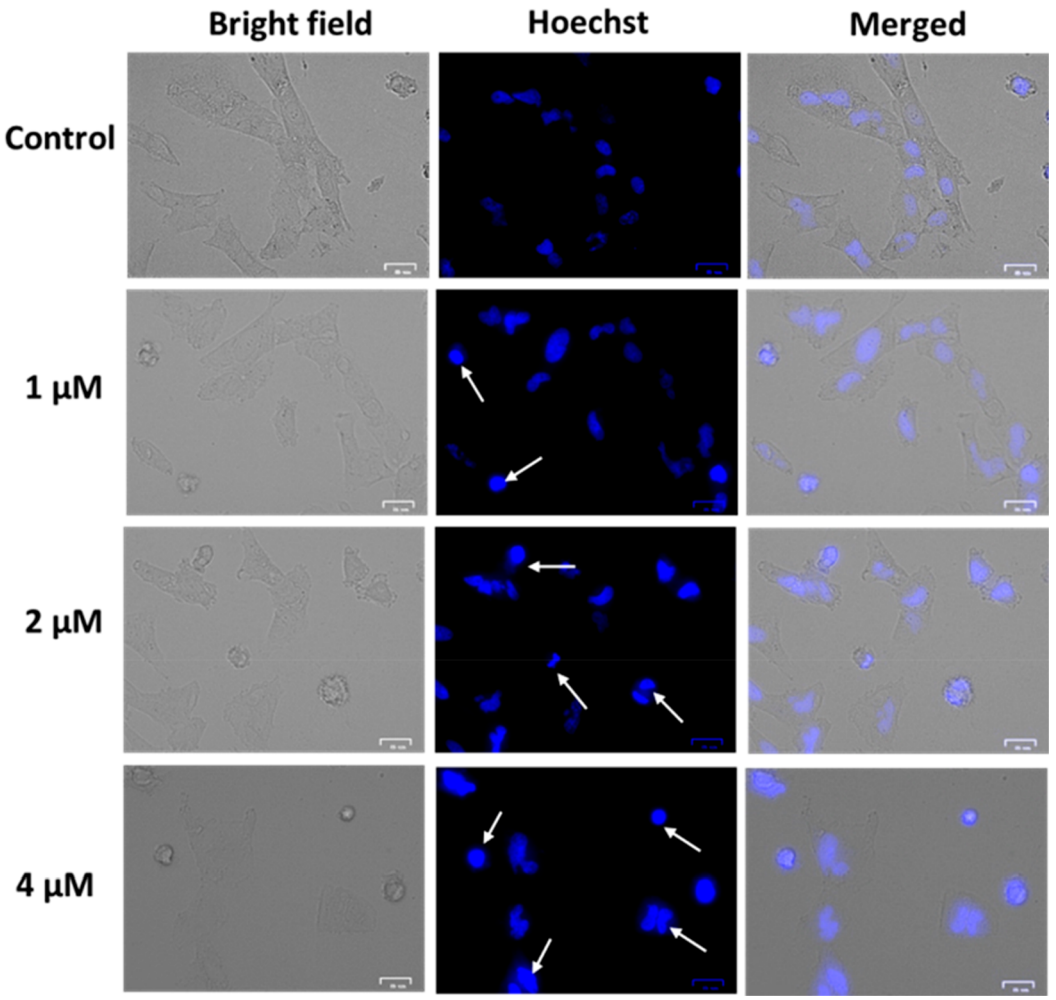

Figure 11. Nuclear morphological changes in the D24 cells after treatment with different concentrations of complex **3c** as determined by Hoechst 33242 staining.

ligands. Replacement of triphenylphosphine by PTA resulted in a reduction of the activity. The most potent compound in the series **3c** displayed antiproliferative activities in the range of 1.53−6.02 μM, comparable to, or better than, cisplatin (0.63−23.5 μM). The cytotoxicity of **3c** was 20-fold higher than that of cisplatin toward D24 melanoma cells. Moreover, 5-fold higher selectivity toward melanoma cells than normal Hek293T cells was observed. The more physiologically relevant 3D tumor spheroidal assays on D24 melanoma cells revealed the cytotoxic potential of **3c**. Anticancer effects in D24 cells were triggered by **3c** through TrxR enzyme inhibition and mitochondrial-mediated apoptosis. Compound **3c** also has significant antiangiogenic effects in zebrafish embryos, in contrast to cisplatin, which is almost inactive at the tested concentrations. In summary, the newly synthesized alkynyl gold complexes of the type (triphenylphosphine)gold-(I) alkyne showed promising potential as future cancer therapeutics.

EXPERIMENTAL SECTION

Chemistry. $[AuCl(PPh_3)]$[38] and $[AuCl(PTA)]$[39] were prepared following literature methods. The other chemicals were purchased and used without further purification. ^{1}H (300 MHz), ^{31}P (121 MHz), and ^{13}C (75 MHz) NMR spectra were obtained as $CDCl_3$ solutions on a Bruker Avance 300 spectrometer at room temperature. Chemical shifts are referenced to residual solvent signals (^{1}H and ^{13}C) or external 85% H_3PO_4 (^{31}P), and coupling constants (J) are given in hertz. Mass spectra were acquired on a PerkinElmer Axion 2 time-of-flight electrospray ionization (ESI) spectrometer. Elemental analyses were carried out by the Chemical Analysis Facility in the Department of Molecular Sciences, Macquarie University, New South Wales, Australia.

X-ray Crystallography. Crystals of complex **3a** suitable for single-crystal X-ray diffraction were obtained from dichloromethane/hexane. A crystal was mounted on a nylon loop using a drop of inert oil (Nujol) before being transferred into a stream of cold nitrogen. The reflections were collected on a D8 Bruker diffractometer equipped with an APEX-II area detector using graphite-monochromated Mo Kα radiation (λ = 0.71073 Å) from a 1 μS microsource. For data collection and data processing, *SMART*[40] and *SAINT*[41] were used, respectively, and absorption corrections were performed using *SADABS*.[42] The structure was solved using direct methods and refined with full-matrix least-squares methods on F^2 using the *SHELX-TL* package.[43,44] The CCDC number for complex **3a** is 1873465.

Synthesis. *General Procedure for the Synthesis of N-(Prop-2-yn-1-yl)cinnamamides (**2a−2c**).* To a solution of substituted cinnamic acid (**1a−1c**; 1.0 mmol) and EDC (1.2 mmol) in anhydrous dimethylformamide were added DIPEA (1.2 mmol) and HOBT (1.2 mmol) at 0 °C under a nitrogen atmosphere. After the reaction mixture was stirred for 10 min, propargylamine (1.0 mmol) was added and stirring continued at room temperature for 12 h. The reaction mixture was poured into ice-cold water (25 mL) and extracted with ethyl acetate (3 × 15 mL). The organic layer was separated, washed with a NaCl solution, and dried over anhydrous Na_2SO_4, and the

DOI: 10.1021/acs.inorgchem.9b00281
Inorg. Chem. XXXX, XXX, XXX−XXX

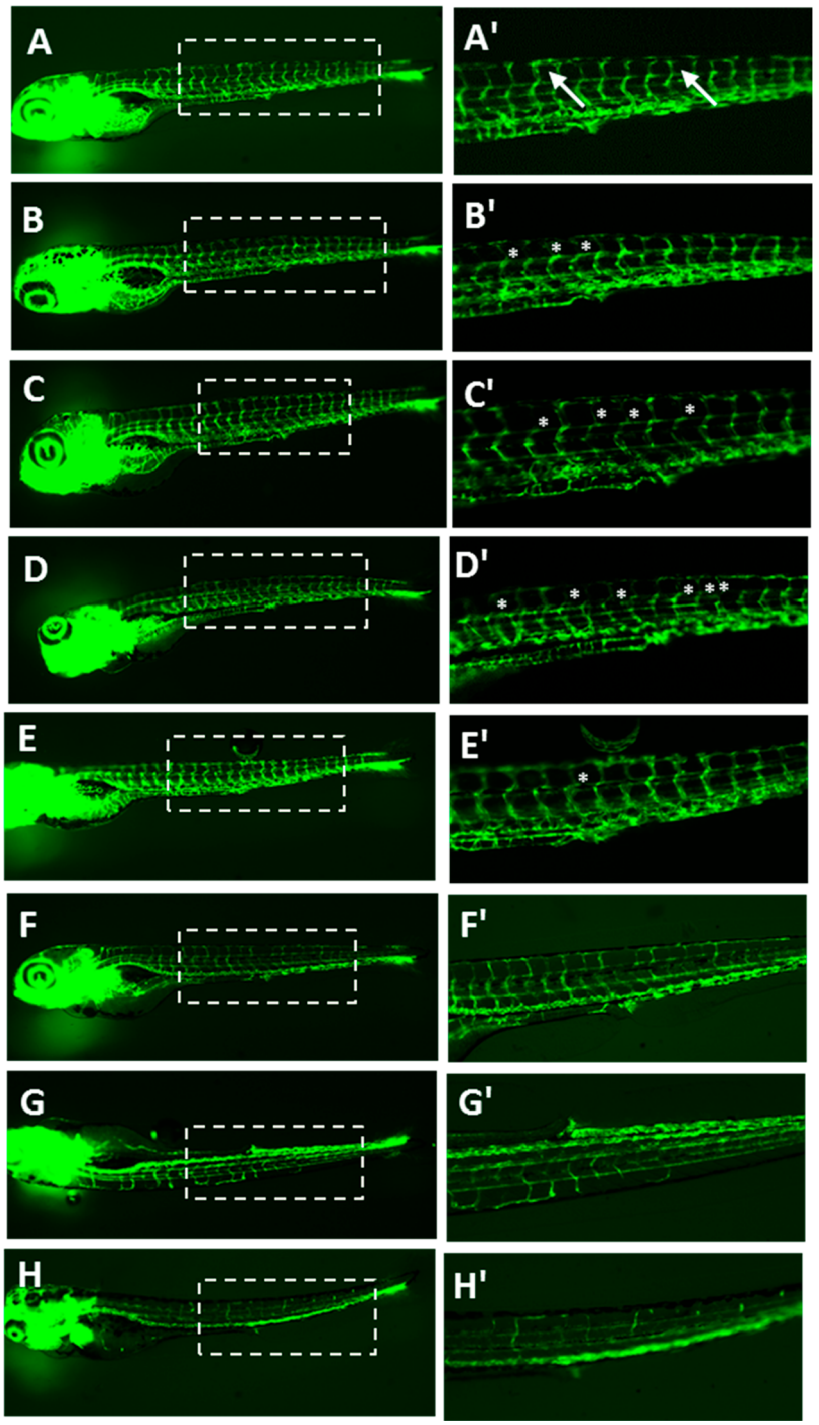

Figure 12. Angiogenesis assay in transgenic *Tg(fli1a:EGFP)* zebrafish embryos. Embryos were treated with different concentrations of compound **3c**, with cisplatin and axitinib as positive controls, at 24 hpf. The images of the zebrafish larvae at 4 dpf were captured using a fluorescence microscope in a green channel: (A and A′) vehicle-treated control embryos; (B−D and B′−D′) compound-**3c**-treated embryos at 0.1, 0.25, and 0.5 μM; (E and E′) cisplatin-treated embryos (1 μM); (F−H and F′−H′) axitinib-treated embryos at 0.1, 0.2, and 0.5 μM concentrations. ISVs are shown by white arrows. Inhibition of ISV sprouting is marked with an asterisk. The magnified portions of images A−H are shown in A′−H′, respectively.

solvent was evaporated. The crude products were purified by column chromatography using ethyl acetate/hexane (30−50%) as the eluent to obtain the desired cinnamide alkynes (**2a**−**2c**) in 75−90% yield.

*(E)-3-(4-Methoxyphenyl)-N-(prop-2-yn-1-yl)acrylamide (**2a**).* ^{1}H NMR: δ 7.65 (d, J = 15.6 Hz, 1H), 7.48 (d, J = 8.7 Hz, 2H), 6.92 (d, J = 8.7 Hz, 2H), 6.30 (d, J = 15.6 Hz, 1H), 5.80 (br s, 1H), 4.22 (dd, J = 5.1 and 2.5 Hz, 2H), 3.87 (s, 3H), 2.29 (t, J = 2.5 Hz, 1H). ^{13}C NMR: δ 165.85, 161.11, 141.63, 129.49, 127.34, 117.30, 114.33, 79.61, 71.75, 55.40, 29.45. ESI-MS: m/z 216.2 ([M + H]$^+$).

*(E)-3-(3,4-Dimethoxyphenyl)-N-(prop-2-yn-1-yl)acrylamide (**2b**).* ^{1}H NMR: δ 7.63 (d, J = 15.6 Hz, 1H), 7.12 (dd, J = 8.3 and 1.8 Hz, 1H), 7.05 (d, J = 1.8 Hz, 1H), 6.89 (d, J = 8.3 Hz, 1H), 6.31 (d, J = 15.6 Hz, 1H), 5.80 (br s, 1H), 4.23 (dd, J = 5.2 and 2.5 Hz, 2H), 3.94 (s, 6H), 2.29 (t, J = 2.5 Hz, 1H). ^{13}C NMR: δ 165.73, 150.83, 149.20,

DOI: 10.1021/acs.inorgchem.9b00281
Inorg. Chem. XXXX, XXX, XXX−XXX

141.85, 127.60, 122.16, 117.57, 111.14, 109.74, 79.57, 71.80, 56.00, 55.92, 29.48. ESI-MS: m/z 246.2 ($[M + H]^+$).

*(E)-N-(Prop-2-yn-1-yl)-3-(3,4,5-trimethoxyphenyl)acrylamide (**2c**).* ^{1}H NMR: δ 7.60 (d, J = 15.5 Hz, 1H), 6.76 (s, 2H), 6.35 (d, J = 15.5 Hz, 1H), 5.87 (br s, 1H), 4.23 (dd, J = 5.0 and 2.5 Hz, 2H), 3.91 (s, 9H), 2.30 (t, J = 2.5 Hz, 1H). ^{13}C NMR: δ 165.45, 153.47, 141.95, 139.83, 130.17, 119.07, 105.08, 79.45, 71.88, 61.00, 56.18, 29.51. ESI-MS: m/z 276.2 ($[M + H]^+$).

*General Procedure for the Synthesis of Gold(I) Alkynes (**3a**–**3c** and **4a**–**4c**).* To a suspension of [AuCl(PPh$_3$)] or [AuCl(PTA)] (1.0 mmol) in methanol were added cinnamide alkynes (**2a**–**2c**, 1.0 mmol) and NaOH (1.1 mmol), and the mixture was stirred for 8 h at room temperature. The precipitated solid was isolated by filtration, washed with methanol and diethyl ether, and dried in vacuo to give the title compounds in good yield (90–95%).

3a. ^{1}H NMR: δ 7.34–7.43 (m, 18H), 6.92 (d, J = 8.6 Hz, 2H), 6.26 (d, J = 15.6 Hz, 1H), 5.78 (br s, 1H), 4.37 (d, J = 4.6 Hz, 2H), 3.86 (s, 3H). ^{31}P NMR: δ 42.12. ESI-MS: m/z 674.3 ($[M + H]^+$). Elem anal. Calcd for $C_{31}H_{27}AuNO_2P$ (673.14): C, 55.28; H, 4.04; N, 2.08. Found: C, 54.66; H, 3.92; N, 1.99.

3b. ^{1}H NMR: δ 7.60–7.44 (m, 15H), 7.10 (dd, J = 8.3 and 1.8 Hz, 1H), 7.04 (d, J = 1.8 Hz, 1H), 6.88 (d, J = 8.3 Hz, 1H), 6.28 (d, J = 15.6 Hz, 1H), 5.83 (br s, 1H), 4.37 (d, J = 4.7 Hz, 1H), 3.93 (s, 6H). ^{13}C NMR: δ 165.49, 150.55, 149.14, 140.79, 134.30, 134.21, 131.66, 129.23, 129.15, 127.93, 121.88, 118.49, 111.12, 109.76, 55.95, 55.91, 31.02. ^{31}P NMR: δ 42.10. ESI-MS: m/z 704.3 ($[M + H]^+$). Elem anal. Calcd for $C_{32}H_{29}AuNO_3P$ (703.15): C, 54.63; H, 4.15; N, 1.99. Found: C, 54.78; H, 3.95; N, 1.97.

3c. ^{1}H NMR: δ 7.60–7.44 (m, 15H), 6.76 (d, J = 5.8 Hz, 2H), 6.31 (d, J = 15.6 Hz, 1H), 5.86 (br s, 1H), 4.37 (d, J = 4.7 Hz, 2H), 3.92 (s, 6H), 3.89 (s, 3H). ^{13}C NMR: δ 165.19, 153.41, 140.94, 134.39, 134.21, 131.67, 130.51, 130.41, 129.97, 129.31, 129.16, 119.94, 104.93, 77.25, 61.00, 56.17, 31.06. ^{31}P NMR: δ 42.06. ESI-MS: m/z 734.3 ($[M + H]^+$). Elem anal. Calcd for $C_{33}H_{31}AuNO_4P$ (733.16): C, 54.03; H, 4.26; N, 1.91. Found: C, 54.31; H, 4.10; N, 1.89.

4a. ^{1}H NMR: δ 7.67–7.51 (m, 1H), 7.47 (d, J = 8.6 Hz, 2H), 6.91 (d, J = 8.7 Hz, 2H), 6.29 (d, J = 15.6 Hz, 1H), 5.99 (br s, 1H), 4.64–4.45 (m, 6H), 4.33–4.25 (m, 8H), 3.86 (s, 3H). ^{13}C NMR: δ 165.65, 160.92, 140.61, 129.38, 127.61, 118.17, 114.30, 73.32, 73.22, 55.39, 52.54, 52.27, 30.88. ^{31}P NMR: δ −51.18. ESI-MS: m/z 569.2 ($[M + H]^+$).

4b. ^{1}H NMR: δ 7.56 (d, J = 15.6 Hz, 1H), 7.14–7.03 (m, 2H), 6.90–6.86 (m, 1H), 6.29 (d, J = 15.6 Hz, 1H), 5.88 (br s, 1H), 4.66–4.48 (m, 6H), 4.34–4.24 (m, 8H), 3.93 (s, 6H). ^{31}P NMR: δ −51.09. ESI-MS: m/z 599.2 ($[M + H]^+$).

4c. ^{1}H NMR: δ 7.59 (d, J = 15.6 Hz, 1H), 6.79 (s, 2H), 6.28 (d, J = 15.6 Hz, 1H), 5.88 (br s, 1H), 4.65–4.47 (m, 6H), 4.44–4.33 (m, 8H), 3.93 (s, 6H), 3.89 (s, 3H). ^{31}P NMR: δ −50.62. ESI-MS: m/z 629.2 ($[M + H]^+$).

Cell Culture. A549 (lung) and D24 (melanoma) cells were maintained in a humidified atmosphere of 5% CO_2 at 37 °C in a RPMI medium, and HT1080 (fibrosarcoma) and Hek293T (normal kidney) cells were grown in Dulbecco's modified Eagle's medium (Gibco, Invitrogen). Both media were supplemented with 10% fetal bovine serum (FBS), 1% penicillin, and streptomycin (1000 U mL^{-1}). All of the cell lines were passaged with 0.25% trypsin/1 mM ethylenediaminetetraacetic acid (EDTA) after reaching 80% confluence and used for the experiments. For cell culture experiments, stock concentrations of the compounds (10 mM) were made in DMSO, and the final working concentrations were prepared in a complete cell growth medium.

MTT Assay. The antiproliferative ability of compounds **2a**–**2c**, **3a**–**3c**, and **4a**–**4c** was investigated using MTT assay. The assay is dependent on the ability of live cells to reduce MTT (Invitrogen) to a purple formazan product, which can be measured spectrophotometrically. In this assay, A549 (lung), D24 (melanoma), HT1080 (fibrosarcoma), and Hek293T cells were plated in 96-well plates at a density of 5000 cells well^{-1} and incubated overnight. For determination of the IC_{50} values, the cells were incubated with different concentrations of compounds in the range of 100–0.001 μM (100 μL well^{-1}). 1% DMSO in a complete growth medium was used as the negative control. After 72 h of incubation, the growth medium containing the compounds was replaced with 100 μL of a 0.5 mg mL^{-1} MTT solution. Incubation was continued for 4 h at 37 °C in the dark. Unreacted MTT was removed, and 100 μL of DMSO was added to each well to dissolve the formazan crystals. The absorbances of the solutions were recorded at 570 nm using a microplate reader (SpectraMax). The absorbance is proportional to the number of living cells, and the IC_{50} values were calculated using *Probit* software.

Cell Viability on 3D Cellular Spheroids. D24 cells (4×10^3 well^{-1}) were cultured in a blackwell plate and grown in a RPMI medium supplemented with 10% FBS for 24 h to allow the formation of 3D cellular spheroids. The formed spheroids were treated with different concentrations of complex **3c** for 72 h, and the effect on spheroidal growth was examined by phase-contrast light microscopy. For live dead staining, the drug-treated spheroids were stained with calcein (2 μM) and propidium iodide (4 μM) for 30 min at room temperature and the images were captured using a fluorescence microscope (Bio-Rad).

DNA Binding Studies. The UV–vis absorption studies were primarily employed to analyze the binding modes of the gold complexes to CT-DNA. In this process, the gold complexes (**3a**–**3c** and **4a**–**4c**) were dissolved in DMSO and then diluted to the desired concentration with Tris-buffered saline (25 μM). The quartz cell was used to carry out spectroscopic titrations by adding increasing concentrations of CT-DNA to a solution of the complex (25 μM), and the spectrum was recorded after each addition using an Agilent Cary 500 spectrophotometer.

DNA Cleavage Studies. The interactions of supercoiled pBR322 plasmid DNA and the complexes were determined by using an agarose gel electrophoresis experiment. In this method, supercoiled pBR322 plasmid DNA (300 ng) in a Tris–HCl buffer (5 mM) with 50 mM NaCl (pH 7.2) was treated with different concentrations of metal complexes (10, 5, and 1 μM), followed by dilution with a Tris–HCl buffer to a total volume of 20 μL with 10% gel loading buffer, i.e., Blue Juice (2 μL). The samples were then incubated at 37 °C for 1 h and loaded onto 1.5% agarose gel containing 1.0 mg mL^{-1} SYBR safe (Thermofischer). Electrophoresis was carried out at 70 V for 60 min in a TBE buffer (Tris-borate EDTA). UV light was used for visualizing the obtained bands, and the images were captured by a Gel Documentation System (Bio-Rad).

Molecular Docking. A docking study was performed using *Molegro Virtual Docker* software version 6. *ChemDraw 2D Ultra* was used for the formation of 2D structures of the compounds. Cleanup of the compounds was done, and the energy was minimized using the *MM2* and *MOPAC* tools of *ChemDraw 3D* to achieve the local energy minima. Human mitochondrial enzyme TrxR (PDB ID: 2J3N) was extracted from the Protein Data Bank (https://www.rcsb.org/) based on the criteria that they had reasonable resolution (≤2.8 Å). The pdb had three small molecules, namely, flavin adenine dinucleotide (FAD), nicotinamide adenine dinucleotide phosphate (NADP), and (4*s*)-2-methyl-2,4-pentanediol (MPD). From the three, MPD was selected as the template for locating the active sites available on chains A and B, and the rest of the structures were removed. The grid resolution was set to 0.30 Å. The cavity was created using the following dimensions while keeping the constraint radius at 14: *X*, −95.32 Å; *Y*, 99.04 Å; *Z*, 34.77 Å. Along with the other assessment parameters used in the default settings, ligand evaluation was done using the Lennard-Jones potential, sp^2–sp^2 torsions, internal hydrogen bond, and internal entropy. The synthesized ligands were imported, and the docking was performed using the template ligand MPD. Because of the stochastic nature of the ligand–protein docking search algorithm, 10 runs were conducted and 10 docking solutions (pose) were retained for each ligand. From the 10 poses, only one pose was extracted based on the higher moldock score, rerank score, and lowest root-mean-square deviation.

Analysis of Intracellular ROS Production. D24 cells were incubated with the control and different concentrations of the gold complex **3c** (1, 2, and 4 μM) for 48 h. After treatment, the cells were washed with PBS, collected by trypsinization, and further incubated

DOI: 10.1021/acs.inorgchem.9b00281
Inorg. Chem. XXXX, XXX, XXX–XXX

with 10 μM carboxy-H_2DCFDA (Invitrogen) for 30 min at 37 °C. Again, the cells were washed with PBS and immediately subjected to flow-cytometry analysis.

Assessment of Mitochondrial Membrane Potential (DΨm). Briefly, D24 cells were untreated or treated with complex **3c** (1, 2, and 4 μM) for 48 h. After treatment, the cells were trypsinized, collected by centrifugation, and then incubated with JC-1 at 37 °C for 20 min. The stained cells were washed with PBS twice and measured by flow cytometry.

Hoechst 33258 Staining. In this experiment, D24 cells were seeded on a 24-well plate at a density of 50000 cells well^{-1}. After overnight incubation, different concentrations of compound **3c** (1, 2, and 4 μM) were added and the cells were further incubated for 48 h. The cells were collected by trypsinization, washed twice, and fixed with 4% paraformaldehyde. The fixed cells were stained with Hoechst 33258 (2 μg mL^{-1} in PBS) for 20 min at 37 °C in the dark. After incubation, the cells were washed with PBS and observed with a fluorescence microscope (Bio-Rad).

In Vivo Angiogenesis Assay. Zebrafish embryos from the *Tg(fil-1:EGFP)* transgenic line, expressing EGFP, were used in this study. Embryos were obtained from natural spawning. Freshly fertilized eggs were collected immediately upon spawning, placed in embryo medium E3 (146 mg L^{-1} NaCl; 6.3 mg L^{-1} KCl; 24.3 mg L^{-1} $CaCl_2$; 40.7 mg L^{-1} $MgSO_4$), and kept at 28.5 ± 0.5 °C.[45] Fertilized embryos were sorted and developmentally staged before any experiments as described earlier.[46] At 1 day post fertilization stage, the embryos were placed in 5 mL of the E3 medium with different concentrations (0.1, 0.25, and 0.5 μM) of **3c** and axitinib and cisplatin (1 μM) in 6-well plates. At least 10 embryos were placed in each well and incubated in the drug solutions for 72 h at 28.5 °C. After the incubation period, hatched embryos were anaesthetized with 0.01% tricaine, immobilized in 1% low-melting agarose gel, and imaged with a fluorescence microscope (Nikon SMZ18) as described earlier.[47]

■ ASSOCIATED CONTENT

Supporting Information

The Supporting Information is available free of charge on the ACS Publications website at DOI: 10.1021/acs.inorgchem.9b00281.

^{1}H and ^{31}P NMR spectra of the newly synthesized complexes (Figures S1−S15) and stability studies in DMSO-d_6 (Figures S16−S21) (PDF)

Accession Codes

CCDC 1873465 contains the supplementary crystallographic data for this paper. These data can be obtained free of charge via www.ccdc.cam.ac.uk/data_request/cif, or by emailing data_request@ccdc.cam.ac.uk, or by contacting The Cambridge Crystallographic Data Centre, 12 Union Road, Cambridge CB2 1EZ, UK; fax: +44 1223 336033.

■ AUTHOR INFORMATION

Corresponding Authors

*E-mail: srinivasareddy.telukutla@rmit.edu.au (T.S.R.).
*E-mail: nedaossadat.mirzadeh@rmit.edu.au (N.M.).
*E-mail: suresh.bhargava@rmit.edu.au (S.B.).

ORCID

T. Srinivasa Reddy: 0000-0002-2806-4300
Steven H. Privér: 0000-0001-5521-9884
Donald Wlodkowic: 0000-0002-0780-3362
Suresh Bhargava: 0000-0002-3127-8166

Notes

The authors declare no competing financial interest.

■ ACKNOWLEDGMENTS

The authors acknowledge the Micro Nano Research Facility, RMIT University, for providing the facilities to carry out cell culture experiments.

■ REFERENCES

(1) WHO: World Health Organization, http://www.who.int/news-room/fact-sheets/detail/cancer (accessed Sept 12, 2018).
(2) Florea, M.; Büsselberg, D. Cisplatin as an anti-tumor drug: cellular mechanisms of activity, drug resistance and induced side effects. *Cancers* **2011**, *3*, 1351−1371.
(3) Gibson, D. The mechanism of action of platinum anticancer agents—what do we really know about it? *Dalton Trans.* **2009**, *48*, 10681−10689.
(4) Ott, I. On the medicinal chemistry of gold complexes as anticancer drugs. *Coord. Chem. Rev.* **2009**, *253*, 1670−1681.
(5) Zou, T.; Lum, C. T.; Lok, C. N.; Zhang, J. J.; Che, C. M. Chemical biology of anticancer gold(III) and gold(I) complexes. *Chem. Soc. Rev.* **2015**, *44*, 8786−8801.
(6) Yeo, C. I.; Ooi, K. K.; Tiekink, E. R. T. Gold-Based Medicine: A Paradigm Shift in Anti-Cancer Therapy? *Molecules* **2018**, *23*, 1410−1435.
(7) Scheffler, H.; You, Y.; Ott, I. Comparative studies on the cytotoxicity, cellular and nuclear uptake of a series of chloro gold(I) phosphine complexes. *Polyhedron* **2010**, *29*, 66−69.
(8) McKeage, M. J.; Berners-Price, S. J.; Galettis, P.; Bowen, R. J.; Brouwer, W.; Ding, L.; Zhuang, L.; Baguley, B. C. Role of lipophilicity in determining cellular uptake and antitumour activity of gold phosphine complexes. *Cancer Chemother. Pharmacol.* **2000**, *46*, 343−350.
(9) Reddy, T. S.; Privér, S. H.; Rao, V. V.; Mirzadeh, N.; Bhargava, S. K. Gold(I) and gold(III) phosphine complexes: synthesis, anticancer activities towards 2D and 3D cancer models, and apoptosis inducing properties. *Dalton Trans.* **2018**, *47*, 15312−15323.
(10) Schuh, E.; Valiahdi, S. M.; Jakupec, M. A.; Keppler, B. K.; Chiba, P.; Mohr, F. Synthesis and biological studies of some gold(I) complexes containing functionalised alkynes. *Dalton Trans.* **2009**, *48*, 10841−10845.
(11) Mirzadeh, N.; Privér, S. H.; Abraham, A.; Shukla, R.; Bansal, V.; Bhargava, S. K. Linking Flavonoids to Gold−A New Family of Gold Compounds for Potential Therapeutic Applications. *Eur. J. Inorg. Chem.* **2015**, *2015*, 4275−4279.
(12) Cozzi, P.; Beria, I.; Biasoli, G.; Caldarelli, M.; Capolongo, L.; Geroni, C.; Mongelli, N. Novel phenyl nitrogen mustard and half-mustard derivatives of distamycin. *Bioorg. Med. Chem. Lett.* **1997**, *7*, 2979−2984.
(13) De, P.; Baltas, M.; Bedos-Belval, F. Cinnamic acid derivatives as anticancer agents-a review. *Curr. Med. Chem.* **2011**, *18*, 1672−703.
(14) Niero, E. L.; Machado-Santelli, G. M. Cinnamic acid induces apoptotic cell death and cytoskeleton disruption in human melanoma cells. *J. Exp. Clin. Cancer Res.* **2013**, *32*, 31−44.
(15) Zhang, J.; Xiao, A.; Wang, T.; Liang, X.; Gao, J.; Li, P.; Shi, T. Effect and mechanism of action of cinnamic acid on the proliferation and apoptosis of leukaemia cells. *Biomed. Res.* **2014**, *25*, 405−408.
(16) Xu, C. C.; Deng, T.; Fan, M. L.; Lv, W. B.; Liu, J. H.; Yu, B. Y. Synthesis and in vitro antitumor evaluation of dihydroartemisinin-cinnamic acid ester derivatives. *Eur. J. Med. Chem.* **2016**, *107*, 192−203.
(17) Reddy, V. G.; Bonam, S. R.; Reddy, T. S.; Akunuri, R.; Naidu, V. G. M.; Nayak, V. L.; Bhargava, S. K.; Kumar, H. M. S.; Srihari, P.; Kamal, A. 4β-amidotriazole linked podophyllotoxin congeners: DNA topoisomerase-IIα inhibition and potential anticancer agents for prostate cancer. *Eur. J. Med. Chem.* **2018**, *144*, 595−611.
(18) Hikisz, P.; Szczupak, L.; Koceva-Chyła, A.; Guśpiel, A.; Oehninger, L.; Ott, I.; Therrien, B.; Solecka, J.; Kowalski, K. Anticancer and Antibacterial Activity Studies of Gold(I)-Alkynyl Chromones. *Molecules* **2015**, *20*, 19699−19718.

DOI: 10.1021/acs.inorgchem.9b00281
Inorg. Chem. XXXX, XXX, XXX−XXX

(19) Gavara, R.; Aguiló, E.; Schur, J.; Llorca, J.; Ott, I.; Rodríguez, L. Study of the effect of the chromophore and nuclearity on the aggregation and potential biological activity of gold(I) alkynyl complexes. *Inorg. Chim. Acta* **2016**, *446*, 189−197.
(20) Sánchez-de-Diego, C.; Mármol, I.; Pérez, R.; Gascón, S.; Rodriguez-Yoldi, M. J.; Cerrada, E. The anticancer effect related to disturbances in redox balance on Caco-2 cells caused by an alkynyl gold(I) complex. *J. Inorg. Biochem.* **2017**, *166*, 108−121.
(21) Mármol, I.; Virumbrales-Muñoz, M.; Quero, J.; Sánchez-de-Diego, C.; Fernández, L.; Ochoa, I.; Cerrada, E.; Yoldi, M. J. R. Alkynyl gold(I) complex triggers necroptosis via ROS generation in colorectal carcinoma cells. *J. Inorg. Biochem.* **2017**, *176*, 123−133.
(22) Wan, X.; Li, Z.; Ye, H.; Cui, Z. Three-dimensional perfused tumour spheroid model for anti-cancer drug screening. *Biotechnol. Lett.* **2016**, *38*, 1389−1395.
(23) Huang, H.; Zhang, P.; Chen, H.; Ji, L.; Chao, H. Comparison between polypyridyl and cyclometalated ruthenium(II) complexes: anticancer activities against 2D and 3D cancer models. *Chem. - Eur. J.* **2015**, *21*, 715−725.
(24) Sunita, M.; Anupama, B.; Ushaiah, B.; Gyana Kumari, C. Synthesis, characterization, DNA binding and cleavage studies of mixed-ligand copper (II) complexes. *Arabian J. Chem.* **2017**, *10*, S3367−S3374.
(25) Kwong, W. L.; Lok, C. N.; Tse, C. W.; Wong, E. L. M.; Che, C. M. Anti-cancer iron(II) complexes of pentadentate N-donor ligands: cytotoxicity, transcriptomics analyses, and mechanisms of action. *Chem. - Eur. J.* **2015**, *21*, 3062−3072.
(26) Vergara, E.; Cerrada, E.; Casini, A.; Zava, O.; Laguna, M.; Dyson, P. J. Antiproliferative Activity of Gold(I) Alkyne Complexes Containing Water-Soluble Phosphane Ligands. *Organometallics* **2010**, *29*, 2596−2603.
(27) Tavares, T. T.; Azevedo, G. C.; Garcia, A.; Carpanez, A. G.; Lewer, P. M.; Paschoal, D.; Müller, B. L.; Dos Santos, H. F.; Matos, R. C.; Silva, H.; Grazul, R. M.; Fontes, A. P. S. Gold (I) complexes with aryl-thiosemicarbazones: molecular modelling, synthesis, cytotoxicity and TrxR inhibition. *Polyhedron* **2017**, *132*, 95−104.
(28) Yokoyama, C.; Sueyoshi, Y.; Ema, M.; Mori, Y.; Takaishi, K.; Hisatomi, H. Induction of oxidative stress by anticancer drugs in the presence and absence of cells. *Oncol. Lett.* **2017**, *14*, 6066−6070.
(29) Dharmaraja, A. T. Role of Reactive Oxygen Species (ROS) in Therapeutics and Drug Resistance in Cancer and Bacteria. *J. Med. Chem.* **2017**, *60*, 3221−3240.
(30) Marzano, C.; Gandin, V.; Folda, A.; Scutari, G.; Bindoli, A.; Rigobello, M. P. Inhibition of thioredoxin reductase by auranofin induces apoptosis in cisplatin-resistant human ovarian cancer cells. *Free Radical Biol. Med.* **2007**, *42*, 872−881.
(31) Suski, J. M.; Lebiedzinska, M.; Bonora, M.; Pinton, P.; Duszynski, J.; Wieckowski, M. R. Relation between mitochondrial membrane potential and ROS formation. *Methods Mol. Biol.* **2012**, *810*, 183−205.
(32) Kumar, N. P.; Sharma, P.; Reddy, T. S.; Shankaraiah, N.; Bhargava, S. K.; Kamal, A. Microwave-assisted one-pot synthesis of new phenanthrene fused-tetrahydrodibenzo-acridinones as potential cytotoxic and apoptosis inducing agents. *Eur. J. Med. Chem.* **2018**, *151*, 173−185.
(33) Bold, R. J.; Termuhlen, P. M.; McConkey, D. J. Apoptosis, cancer and cancer therapy. *Surg. Oncol.* **1997**, *6*, 133−142.
(34) Senwar, K. R.; Reddy, T. S.; Thummuri, D.; Sharma, P.; Bharghava, S. K.; Naidu, V. G. M.; Shankaraiah, N. Design and synthesis of 4′-O-alkylamino-tethered-benzylideneindolin-2-ones as potent cytotoxic and apoptosis inducing agents. *Bioorg. Med. Chem. Lett.* **2016**, *26*, 4061−4069.
(35) Streicher, K. L.; Sylte, M. J.; Johnson, S. E.; Sordillo, L. M. Thioredoxin reductase regulates angiogenesis by increasing endothelial cell-derived vascular endothelial growth factor. *Nutr. Cancer* **2004**, *50*, 221−231.
(36) Meyer, A.; Bagowski, C. P.; Kokoschka, M.; Stefanopoulou, M.; Alborzinia, H.; Can, S.; Vlecken, D. H.; Sheldrick, W. S.; Wölfl, S.; Ott, I. On the Biological Properties of Alkynyl Phosphine Gold(I)-Complexes. *Angew. Chem., Int. Ed.* **2012**, *51*, 8895−8899.
(37) Lawson, N. D.; Weinstein, B. M. In vivo imaging of embryonic vascular development using transgenic zebrafish. *Dev. Biol.* **2002**, *248*, 307−318.
(38) Adé, A.; Cerrada, E.; Contel, M.; Laguna, M.; Merino, P.; Tejero, T. Organometallic gold(III) and gold(I) complexes as catalysts for the 1,3-dipolar cycloaddition to nitrones: synthesis of novel gold−nitrone derivatives. *J. Organomet. Chem.* **2004**, *689*, 1788−1795.
(39) Assefa, Z.; McBurnett, B. G.; Staples, R. J.; Fackler, J. P., Jr; Assmann, B.; Angermaier, K.; Schmidbaur, H. Syntheses, Structures, and Spectroscopic Properties of Gold(I) Complexes of 1,3,5-Triaza-7-phosphaadamantane (TPA). Correlation of the Supramolecular Au···Au Interaction and Photoluminescence for the Species (TPA)AuCl and [(TPA-HCl)AuCl]. *Inorg. Chem.* **1995**, *34*, 75−83.
(40) *SMART software version 5.625 for the CCD Detector System*; Bruker AXS Inc.: Madison, WI, 2001.
(41) *SAINTPLUS software version 6.22 for the CCD Detector System*; Bruker AXS Inc.: Madison, WI, 2001.
(42) Blessing, R. H. An Empirical Correction for Absorption Anisotropy. *Acta Crystallogr., Sect. A: Found. Crystallogr.* **1995**, *51*, 33−38.
(43) Sheldrick, G. M. *SHELXTL*, version 2013/4; Universität Göttingen: Göttingen, Germany, 2013.
(44) Sheldrick, G. M. A short history of SHELX. *Acta Crystallogr., Sect. A: Found. Crystallogr.* **2008**, *64*, 112−122.
(45) Akagi, J.; Khoshmanesh, K.; Hall, C. J.; Cooper, J. M.; Crosier, K. E.; Crosier, P. S.; Wlodkowic, D. Fish on chips: Microfluidic living embryo array for accelerated in vivo angiogenesis assays. *Sens. Actuators, B* **2013**, *189*, 11−20.
(46) Zhu, F.; Wigh, A.; Friedrich, T.; Devaux, A.; Bony, S.; Nugegoda, D.; Kaslin, J.; Wlodkowic, D. Automated Lab-on-a-Chip Technology for Fish Embryo Toxicity Tests Performed under Continuous Microperfusion (μFET). *Environ. Sci. Technol.* **2015**, *49*, 14570−14578.
(47) Friedrich, T.; Douek, A. M.; Vandestadt, C.; Wlodkowic, D.; Kaslin, J. A Modular Millifluidic Homeostatic Imaging Plate for Imaging of Larval Zebrafish. *Zebrafish* **2019**, *16*, 37.

DOI: 10.1021/acs.inorgchem.9b00281
Inorg. Chem. XXXX, XXX, XXX−XXX